

**Phonon attenuation and quasiparticle–phonon energy transfer in *d*-wave superconductors**

M. F. Smith and M. B. Walker

*Department of Physics, University of Toronto, Toronto, Ontario, Canada M5S 1A7*

(Received 18 April 2002; revised manuscript received 10 January 2003; published 10 June 2003)

We calculate the rate of energy transfer between phonons and quasiparticles that are out of thermal equilibrium in cuprate superconductors at temperatures below the impurity scattering rate. Phonons that give a significant contribution to phonon-quasiparticle energy transfer at millikelvin temperatures have frequencies that extend through the crossover frequency at which sound attenuation deviates from an  $\omega^2$  frequency dependence. The crossover frequency for a given phonon depends on the direction of its in-plane momentum because of the anisotropy of the nodal quasiparticle energy dispersion relation. The temperature dependence of the heat transfer rate is thus sensitive to the ratio  $v_f/v_2$ , which characterizes the anisotropy of quasiparticle energy at the node. We estimate the magnitude of the heat transfer rate in optimally doped  $\text{YBa}_2\text{Cu}_3\text{O}_{6+x}$ . We also compare our results for pure *d*-wave superconductors with measurements of the ultrasonic attenuation in  $\text{Sr}_2\text{RuO}_4$  and discuss implications for the gap symmetry in that material.

DOI: 10.1103/PhysRevB.67.214509

PACS number(s): 74.25.Ld, 74.25.Fy

**I. INTRODUCTION**

This paper develops a model describing the attenuation of sound waves in the cuprate superconductors such as  $\text{YBa}_2\text{Cu}_3\text{O}_{6+x}$ , and makes use of the results to develop a theory of heat transfer between the Bogoliubov quasiparticle excitations (called simply quasiparticles in what follows) and phonons (which will not be called quasiparticles in this paper). In the attenuation of phonons in normal metals, it is well known<sup>1</sup> that there exist two distinct physical regimes, a low-frequency regime in which the attenuation varies as  $\omega^2$ , the square of the phonon frequency, and a high-frequency regime where the attenuation varies linearly with the phonon frequency. The crossover between these two regimes occurs when the electron mean free path  $\ell$  is equal to the phonon wavelength.

One of the remarkable results of this article is that the crossover frequency at which the attenuation deviates from low-frequency  $\omega^2$  behavior is extremely anisotropic at low temperatures in a *d*-wave superconductor such as  $\text{YBa}_2\text{Cu}_3\text{O}_{6+x}$ , so that, for example, a longitudinal phonon propagating in the [100] direction crosses over at a much lower frequency (by a factor of more than 10) than does a longitudinal phonon propagating in the [110] direction. This strong anisotropy comes from the strong anisotropy of the velocity of the nodal quasiparticles in a *d*-wave superconductor. The energy of a low-energy nodal quasiparticle in a *d*-wave superconductor can be written as<sup>2</sup>

$$E_{\mathbf{k}} = \sqrt{(\hbar v_f k_1)^2 + (\hbar v_2 k_2)^2}, \quad (1)$$

where  $k_1$  and  $k_2$  are measured from the nodal point, and  $k_1$  is measured perpendicular to the Fermi surface, while  $k_2$  is measured parallel to the Fermi surface. The ratio of the velocity perpendicular to the Fermi surface,  $v_f$ , to that parallel to the Fermi surface,  $v_2$ , is approximately 15 in  $\text{YBa}_2\text{Cu}_3\text{O}_{6+x}$ .<sup>3</sup> Now, we define the mean free path of a nodal quasiparticle in a given direction to be its group velocity in that direction, times its inverse scattering rate (assumed independent of direction), so that this mean free path can

vary by a factor of roughly 15 in  $\text{YBa}_2\text{Cu}_3\text{O}_{6+x}$ , according to whether the quasiparticle is traveling parallel or perpendicular to the Fermi surface (motion in the [001] plane only is assumed). As noted above, the crossover from low-frequency to high-frequency behavior occurs when the quasiparticle mean free path is equal to the phonon wavelength, and it is the quasiparticle mean free path in the direction of phonon propagation that is relevant in the anisotropic case studied here. This qualitative explanation for the strong anisotropy predicted for the crossover from low frequency to high-frequency behavior will be developed quantitatively in some detail in the body of this paper.

In this paper, the range of sound wave frequencies, for a given sound wave polarization and direction, over which the sound wave attenuation varies as  $\omega^2$ , will be the low-frequency regime. [The term hydrodynamic regime, often used to describe the region of an  $\omega^2$  dependence of the attenuation (e.g., see Ref. 4), will not be used in this paper.]

According to the quantitative estimates given below, the crossovers that are expected to occur in  $\text{YBa}_2\text{Cu}_3\text{O}_{6+x}$  from a low-frequency  $\omega^2$  behavior to a distinctive behavior at higher frequency occur at too high a frequency to be observable in standard ultrasonic attenuation experiments. The strong anisotropy of the crossover frequency has, however, a significant effect on the temperature dependence of the low-temperature heat transfer between the quasiparticles and the phonons, as will be shown in more detail below.

The rate of energy transfer between electrons and phonons has been measured in a normal metal at millikelvin temperatures.<sup>5,6</sup> In these experiments, performed on thin metal films deposited on insulating substrates, the electrons in the metal were heated by an applied current, and came into thermal equilibrium at a temperature  $T_{el}$  via electron-electron scattering. Phonon-phonon interactions occurring mainly within the substrate allowed the phonons in the metal to remain in thermal equilibrium at a temperature  $T_{ph}$ . A significant difference between the electron and phonon equilibrium temperatures was maintained by the applied current. A steady power transfer from the electrons to the phonons was thus established. In the calculations of heat transfer in

this article we also assume that the electron and phonon systems in the film can be characterized by their respective temperatures,  $T_{el}$  and  $T_{ph}$ . This should be recognized as a basic assumption of our work, which we do not attempt to justify by detailed calculation.

As in the related problem of sound attenuation in metals, the behavior of electron-phonon heat transfer depends on the relative size of the average phonon wave vector  $q = \hbar\omega/c_s$  and the electronic mean free path  $\ell = v_f/\Gamma$  where  $c_s$  is the speed of sound. The phonon wave vector is fixed by a transducer in sound attenuation experiments, and determined by the phonon temperature  $T_{ph}$  in the heat transfer problem. In high frequency ultrasound experiments performed on clean metals, the clean (or quantum) limit defined by  $q\ell \gg 1$ , may be attained. In this limit, the sound attenuation varies linearly with phonon frequency and the corresponding electron-phonon heat transfer rate is proportional to  $T_{ph}^5 - T_{el}^5$ . As the frequency is decreased, the attenuation crosses over to the low-frequency limit for which  $q\ell \ll 1$ . The sound attenuation is then proportional to  $\omega^2$  and the heat transfer rate varies as  $T_{ph}^6 - T_{el}^6$ .

The problem of calculating the energy transfer rate between phonons and an electron gas at different temperatures has been previously studied.<sup>5,7</sup> In this paper, we calculate the energy transfer rate between phonons and quasiparticles which are at different equilibrium temperatures in the millikelvin range. Evidence for the validity of the  $d$ -wave nodal quasiparticle picture at low temperature in optimally doped cuprates is provided by measurements of numerous thermodynamic and transport properties.<sup>8-14</sup> At temperatures far below  $T_c$  the number of thermally activated quasiparticles and the quasiparticle-quasiparticle scattering rate are small. However the density of states of the quasiparticles is linear for energy above  $\hbar\Gamma$  and constant for energy less than  $\hbar\Gamma$ ,<sup>2</sup> whereas the phonon density of states varies quadratically with the phonon energy. So the number of thermally excited phonons decreases faster with temperature than the number of excited nodal quasiparticles. At sufficiently low temperatures, there will be many less quasiparticle-phonon collisions than quasiparticle-quasiparticle collisions, and we expect that the quasiparticles will reach thermal equilibrium with each other before reaching equilibrium with the phonons, as do the electrons in a normal metal.

Calculations of the sound attenuation and electron-phonon heat transfer depend on the assumed form of the electron-phonon matrix element. In tight-binding materials with square lattices, such as the cuprate and ruthenate superconductors, the lattice geometry plays a crucial role in the electron-phonon interaction. A form for the interaction which is appropriate in such materials has recently been developed,<sup>15</sup> and shown to account for the unusual normal state attenuation of  $\text{Sr}_2\text{RuO}_4$ .<sup>16</sup> This interaction, which depends on a single parameter characterizing the coupling strength, will be employed here. A measurement made of either the electron-phonon heat transfer or acoustic attenuation in a cuprate material will fix the value of the coupling and thus determine the magnitude of the other quantity. Ultrasonic attenuation studies of cuprate materials have not been performed because crystal samples of sufficient size are

not yet available. To make a rough estimate of the expected magnitude of the heat transfer rate in cuprates, we will use the value for the electron-phonon coupling determined for  $\text{Sr}_2\text{RuO}_4$ .

## II. ULTRASONIC ATTENUATION IN $d$ -WAVE SUPERCONDUCTORS FOR $T < \Gamma$

The rate of heat transfer between phonons at a temperature  $T_{ph}$  and electrons at a temperature  $T_{el}$  is given by<sup>7</sup>

$$\frac{dU}{dt} = \sum_{\mathbf{q}j} \hbar\omega_{\mathbf{q}j} \frac{1}{\tau_{\mathbf{q}j}} \left[ n \left( \frac{\hbar\omega_{\mathbf{q}j}}{k_B T_{ph}} \right) - n \left( \frac{\hbar\omega_{\mathbf{q}j}}{k_B T_{el}} \right) \right], \quad (2)$$

where the sum is taken over all phonon states of wave vector  $\mathbf{q}$ , mode  $j$ , and energy  $\hbar\omega_{\mathbf{q}j}$ ,  $\tau_{\mathbf{q}j}$  is the phonon lifetime, and  $n(x)$  is a Bose factor at the indicated temperature. The calculation of the phonon lifetime for a given momentum and polarization is outlined below. The sound attenuation for a phonon of wave vector  $\mathbf{q}$  and polarization  $j$  is equal to the inverse of the product of the phonon lifetime and sound velocity, i.e.,  $\alpha_{\mathbf{q}j} = (c_{\mathbf{q}j}\tau_{\mathbf{q}j})^{-1}$ . This result, which is intuitively clear, can also be derived from a linear response treatment of sound wave propagation.<sup>17</sup>

We consider phonons with frequencies which are small compared to the impurity scattering rate,  $\omega/\Gamma < 1$  but with wavelengths which are not necessarily small compared to the quasiparticle mean-free path. That is, we allow  $\omega v_g/(c_s\Gamma)$  to be much greater than unity, where  $v_g = |dE/d(\hbar\mathbf{k})|$  is the group velocity of a quasiparticle at a node and  $c_s$  is the speed of sound. This covers phonon frequencies which contribute significantly to heat transfer at temperatures for which  $k_B T/\Gamma < 0.1$  or so. The attenuation in  $d$ -wave superconductors at temperatures above  $\Gamma$  has previously been investigated in both the clean<sup>18</sup> and low-frequency limits.<sup>4,19</sup>

We use the imaginary part of the phonon self energy calculated using superconducting Green's functions with a constant self energy part due to scattering from position-averaged impurities. We omit vertex corrections for simplicity and obtain

$$\begin{aligned} \tau_{\mathbf{q}j}^{-1} = & \frac{8g^2\omega_{\mathbf{q}}}{\rho c_{\mathbf{q}j}^2 \Omega} \sum_{\mathbf{k}} \int dx f_j^2(\mathbf{q}, \mathbf{k}) (n_f(x^-) - n_f(x^+)) \\ & \times (\text{Im}G^R(\mathbf{k}', x^+) \text{Im}G^R(\mathbf{k}, x^-) \\ & - \text{Im}F^R(\mathbf{k}', x^+) \text{Im}F^R(\mathbf{k}, x^-)) \end{aligned} \quad (3)$$

where  $x^\pm = x \pm \omega/2$ ,  $\mathbf{k}' = \mathbf{k} + \mathbf{q}$ ,  $n_f(x)$  is the Fermi function, and  $G^R(\mathbf{k}, x)$ ,  $F^R(\mathbf{k}, x)$  are the normal and anomalous retarded Green's functions for a  $d$ -wave superconductor with an impurity scattering rate  $\Gamma$  and no other self-energy corrections. The electron-phonon interaction for electrons in the copper-oxide plane is described by the coupling constant  $g$  and the function

$$f_j(\mathbf{q}, \mathbf{k}) = \sum_{\mathbf{R}} (\hat{\mathbf{q}} \cdot \hat{\mathbf{R}}) [\hat{\mathbf{R}} \cdot \mathbf{e}_j(\mathbf{q})] \cos(\mathbf{k} \cdot \mathbf{R}) \quad (4)$$

for a phonon of wave vector  $\mathbf{q}$  and polarization vector  $\mathbf{e}_j(\mathbf{q})$  with the sum carried out over the four nearest-neighbor planar

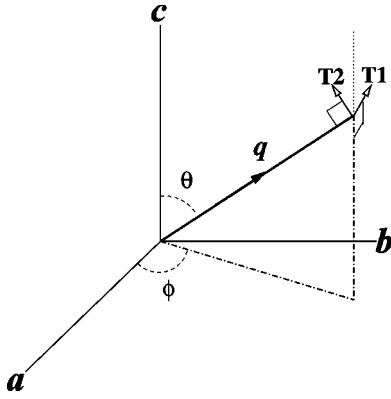


FIG. 1. The orientation of the phonon wave vector with respect to the crystal axes. The polarization vectors labeled T1 and T2 describe the two independent transverse modes. The T1 (T2) polarization vector is perpendicular (parallel) to the plane on which  $\mathbf{q}$  and the  $\mathbf{c}$  axis lie.

sites  $\mathbf{R}$ . This form of the interaction is identical to that used to describe the nearest-neighbor,  $\gamma$ -band interaction in  $\text{Sr}_2\text{RuO}_4$ .<sup>15</sup>

After neglecting terms of order the temperature or the phonon frequency we carry out the energy integration and obtain a simple expression for the inverse phonon lifetime,

$$\frac{1}{\tau_{\mathbf{q},j}} = \frac{8(\hbar\omega_{\mathbf{q},j})^2 g^2}{\rho c_{\mathbf{q},j}^2 \Omega} \sum_{\mathbf{k}} \frac{(\hbar\Gamma)^2 f_j^2(\mathbf{q},\mathbf{k})}{[E_{\mathbf{k}}^2 + (\hbar\Gamma)^2][E_{\mathbf{k}+\mathbf{q}}^2 + (\hbar\Gamma)^2]}. \quad (5)$$

Equation (5) agrees with the result of numerical integration of the more general expression, Eq. (3), over the tem-

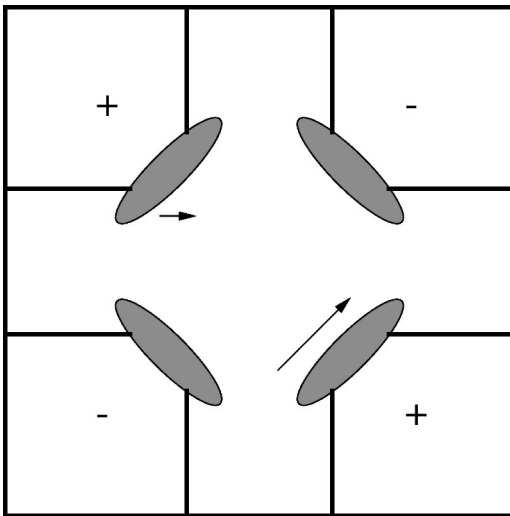


FIG. 2. A typical Fermi surface for a cuprate superconductor. The nodes are labeled as + or - in accordance with Eq. (7) and the shaded region at each node is bounded by the energy contour  $E_{\mathbf{k}} = \Gamma$ . Phonon wave vectors in the 100 and 110 directions are indicated by the arrows located near a node. These vectors have lengths sufficient to span the shaded region of the nearby node, corresponding to the maximum phonon frequencies falling within the low-frequency regime.

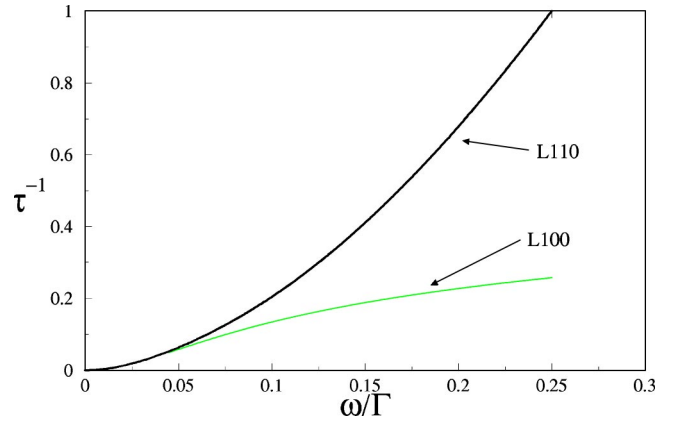


FIG. 3. The normalized phonon relaxation rate as a function of frequency for the L100 and L110 modes at low temperature. The L110 lifetime is nearly proportional to  $\omega^2$  over the range shown. The L100 lifetime crosses over from  $\omega^2$  to a logarithmic behavior at  $\omega/\Gamma \approx c_s/v_f$ .

perature and frequency ranges considered here. Equation (5) is not applicable for temperatures or phonon frequencies approaching the impurity scattering rate.

We first consider longitudinal phonons in the  $\theta, \phi$  direction with respect to the  $\hat{\mathbf{x}} = \hat{\mathbf{a}}$  and  $\hat{\mathbf{z}} = \hat{\mathbf{c}}$  crystal axes as shown in Fig. 1. Then

$$f_j(\mathbf{q},\mathbf{k}) = 2 \sin^2(\theta) [\cos(k_x a) \cos^2(\phi) + \cos(k_y a) \sin^2(\phi)], \quad (6)$$

which, for quasiparticles at the nodes of a  $d_{x^2-y^2}$  gap reduces to  $f_j(\mathbf{q},\mathbf{k}) = 2 \sin^2(\theta) \cos(k_n a)$  where  $\sqrt{2}k_n$  is the length of the wave vector to a node. We take the sound velocity to be isotropic, which is roughly the case in cuprate and ruthenate materials. For example, resonant ultrasonic measurements made of the elastic constants of  $\text{YBa}_2\text{Cu}_3\text{O}_{6+x}$  (Ref. 20) and  $\text{Sr}_2\text{RuO}_4$  (Ref. 21) indicate that the longitudinal sound velocity does not vary significantly with direction (the same is true for transverse phonons). The factor  $E_{\mathbf{k}+\mathbf{q}}^2$  in the denominator of Eq. (5) is thus responsible for any significant planar anisotropy of the phonon relaxation rate. Since  $k_B T < \hbar\Gamma \ll \Delta_{max}$ , the sum over states in Eq. (5) is replaced by a sum over the nodes and an integral over small nodal neighborhoods. The nodes, labeled + or -, as indicated in Fig. 2, can give different contributions to the attenuation.

At the lowest phonon frequencies,  $E_{\mathbf{k}} - E_{\mathbf{k}+\mathbf{q}} \ll \Gamma$  so the  $\mathbf{q}$  dependence in the denominator of Eq. (5) can be ignored and the low-frequency limit, with the characteristic  $\omega^2$  dependence of the relaxation rate, is recovered. The phonon relaxation rate in the low-frequency limit is independent of  $\Gamma$ , and hence of the impurity concentration. At higher frequencies, according to Eq. (5), quasiparticles which contribute to the attenuation of a phonon of wave vector  $\mathbf{q}$  are those for which neither  $E_{\mathbf{k}}$  nor  $E_{\mathbf{k}+\mathbf{q}}$  significantly exceed  $\Gamma$ . Thus the quasiparticle energy is conserved to within  $\Gamma$  during phonon absorption. This condition is represented in Fig. 2 as the requirement that both  $\mathbf{k}$  and  $\mathbf{k} + \mathbf{q}$  lie within one of the shaded regions bounded by the elliptical energy contour  $E_{\mathbf{k}} = \Gamma$ . The condition is applied to each node separately. The presence of the phonon wave vector in the denominator of Eq. (5) be-

comes significant when its norm  $|\mathbf{q}|$  becomes comparable to the length of the shaded region in the  $\hat{\mathbf{q}}$  direction. This determines the crossover frequency between the low-frequency regime and an intermediate regime in which the attenuation increases more slowly than  $\omega^2$ . Due to the elliptical shape of the quasiparticle energy contours, this crossover frequency strongly depends on the phonon direction.

Using the nodal quasiparticle energy dispersion we have<sup>18</sup>

$$E_{\mathbf{k}+\mathbf{q},\pm}^2 = E_{\mathbf{k}}^2 + 2A_{\pm}E_{\mathbf{k}} + B_{\pm}^2, \quad (7)$$

where

$$A_{\pm} = C \left[ \frac{v_f}{c_s} \cos\left(\phi \pm \frac{\pi}{4}\right) \frac{\xi_k}{E_k} \pm \frac{v_2}{c_s} \sin\left(\phi \pm \frac{\pi}{4}\right) \frac{\Delta_k}{E_k} \right],$$

$$B_{\pm}^2 = C^2 \left\{ \left[ \frac{v_f}{c_s} \cos\left(\phi \pm \frac{\pi}{4}\right) \right]^2 + \left[ \frac{v_2}{c_s} \sin\left(\phi \pm \frac{\pi}{4}\right) \right]^2 \right\}, \quad (8)$$

$$C = \hbar \omega_{\mathbf{q},j} \sin(\theta).$$

The subscript  $\pm$  labels the nodes as in Fig. 2. The result for the L100 and L110 modes are shown in Fig. 3, where values of  $v_f/c_s=45$  and  $v_2/c_s=3$  have been used.

For the L100 phonon, each node makes the same contribution to the relaxation rate. The total relaxation rate crosses over from  $\omega^2$  to a sublinear behavior at a frequency of roughly  $\omega \approx \sqrt{2}c_s/v_f\Gamma = 0.02\Gamma$ , i.e., when the phonon wave vector spans the shaded region at each node in the  $\mathbf{x}$  direction. At very low frequencies, the L110 phonon relaxation also receives equal contributions from the  $+$  and  $-$  nodes. The  $-$  node contribution behaves similarly to the L100 relaxation rate, with a crossover frequency of  $\Gamma c_s/v_f$ . A feature in the L110 attenuation occurs at the  $-$  node crossover frequency, which cannot be seen on the scale of Fig. 3. The major axis of the  $+$  node elliptical contour is parallel to the wave vector of the L110 phonon, so the associated crossover occurs at a frequency of  $\omega \approx \Gamma c_s/v_2 = .3\Gamma$ . For frequencies greater than  $\Gamma c_s/v_f$  the  $+$  nodes give the dominant contribution to the relaxation rate. Consequently, the L110 attenuation shows roughly  $\omega^2$  dependence over the entire range of the plot as seen in Fig. 3.

We contrast the longitudinal attenuation shown in Fig. 3 with the experimental result found for  $\text{Sr}_2\text{RuO}_4$ .<sup>16</sup> The attenuation of the L100 and L110 phonons at the lowest frequencies in Fig. 3 are identical. The coefficient in front of the  $\omega^2$  in the attenuation is the same for both directions because it is determined by the magnitude of the electron-phonon matrix element at the node of the  $d_{x^2-y^2}$  gap, which is independent of  $\phi$  according to Eq. (6) (in which only nearest neighbor interactions are included). The values of the matrix element at points away from the zone diagonals do depend on  $\phi$ . For example, at the nodal points of a gap with  $d_{xy}$  symmetry, which lie on the  $k_x$  and  $k_y$  axes, the matrix elements are different for L100 and L110 phonons. Thus the low-frequency attenuation in a  $d_{xy}$  superconductor is expected to be anisotropic. The most extreme anisotropy of the matrix element occurs close to the  $(\pi/a,0)$  points on the Brillouin zone boundary, at which the matrix element with near-

est neighbor interactions for L110 phonons vanishes while that for L100 phonons remains finite.

The ultrasonic attenuation measurements made by Lupien *et al.* on  $\text{Sr}_2\text{RuO}_4$  were performed within the low-frequency limit as indicated by the  $\omega^2$  behavior reported by the author. The attenuation of longitudinal phonons showed extreme anisotropy in the normal state (the L100 attenuation was roughly 30 times greater than the L110 attenuation) which was found to be due to a difference in the averages over the  $\gamma$  sheet of the  $\text{Sr}_2\text{RuO}_4$  Fermi surface of the electron phonon matrix elements for the two modes.<sup>15</sup> The degree of anisotropy of longitudinal attenuation in materials for which the electron-phonon interaction of Eq. (4) applies is thus dependent on the detailed shape of the Fermi surface. We found, for example, that the Fermi surface of optimally doped  $\text{YBa}_2\text{Cu}_3\text{O}_{6+x}$  (Ref. 22) does not give rise to a significant difference between the L100 and L110 normal state attenuation rates. The  $\gamma$ -sheet of the  $\text{Sr}_2\text{RuO}_4$  Fermi surface comes very close to the  $(\pi/a,0)$  point.<sup>24</sup> The observed anisotropy of the attenuation was found to be due to the contribution to the Fermi surface average coming from the portion of the Fermi surface lying near to  $(\pi/a,0)$ , at which the magnitude of the matrix element for L110 phonons is very small.

As the temperature in the experiment on  $\text{Sr}_2\text{RuO}_4$  was reduced to well below  $T_c$  the attenuation decreased but the ratio of the L110 and L100 attenuation rates remained nearly constant. At temperatures well below  $T_c$ , the attenuation rate in an unconventional superconductor is proportional to an average of the squared electron-phonon matrix element over the portion of the Fermi surface lying near the nodes in the gap. The Fermi surface of  $\text{Sr}_2\text{RuO}_4$  is nearly independent of momentum parallel to the  $\mathbf{c}$  axis.<sup>23,24</sup> The fact that the ratio of the L110 and L100 attenuation rates is independent of temperature thus has a natural explanation if the only nodes in the order parameter are horizontal line nodes (perpendicular to the  $\mathbf{c}$  axis). In that case, as temperature was decreased below  $T_c$ , the region of momentum-space occupied by quasiparticles would shrink along the  $\mathbf{c}$  direction and the ratio of Fermi surface averages of matrix elements for different sound modes would remain the same.

If the gap in  $\text{Sr}_2\text{RuO}_4$  had vertical line nodes in the  $[110]$  planes, corresponding to a  $d_{x^2-y^2}$  symmetry, then the magnitude of the low-temperature longitudinal attenuation rates in the low-frequency limit would be equal for 100 and 110 directions as in Fig. 3 (again, only nearest-neighbor effects are considered). Above  $T_c$  the L100 attenuation would be 30 times larger than the L110 attenuation due to the difference in the Fermi surface average of the matrix elements described above. The L100 attenuation would thus be expected to fall off much faster than the L110 attenuation as the temperature was reduced below  $T_c$  if the gap in  $\text{Sr}_2\text{RuO}_4$  had a  $d_{x^2-y^2}$  symmetry.

Alternatively, if the gap in  $\text{Sr}_2\text{RuO}_4$  had  $d_{xy}$  symmetry, with vertical line nodes in the  $[100]$  planes, then the L110 attenuation would decrease much faster than the L100 attenuation as the temperature fell below  $T_c$ . The anisotropy of the attenuation would be much greater at low temperatures than in the normal state. This would occur because as the temperature was lowered below  $T_c$ , the quasiparticles would

become restricted to that portion of the Fermi surface in which the anisotropy of the electron-phonon matrix element is the greatest: the portion closest to the  $(\pi/a, 0)$  point. Using the tight-binding parameters for the  $\gamma$ -sheet found in Ref. 24, we find that the low-temperature attenuation due to quasiparticles at the nodes of a  $d_{xy}$  gap would be 400 times larger for L100 phonons than for L110 phonons (compared to only 30 times larger at  $T_c$ ). It is clear that if the gap had  $d_{xy}$  symmetry than the ratio of the L100 attenuation to the L110 attenuation would rapidly increase as the temperature was lowered below  $T_c$ .

We see that the constant ratio of the L100 and L110 attenuation rates from the normal state to temperatures far below  $T_c$  is consistent with the result expected for an order parameter with horizontal line nodes but incompatible with that predicted for gaps with vertical line nodes in the [110] or [100] planes. Order parameters having only vertical line nodes can also be ruled out for this material by consideration of transverse attenuation rates.<sup>15</sup>

The two independent transverse modes for the tetragonal crystal are shown in Fig. 1. The nearest-neighbor electron-phonon interaction depends on the  $ab$ -plane projections of the phonon polarization and momentum vectors. Using Eq. (4) for the T1 polarization indicated on Fig. 1, we find for the electron phonon interaction

$$f^{T1}(\mathbf{q}, \mathbf{k}) = 2 \sin^2(\theta) \cos(\phi) \sin(\phi) [\cos(k_x a) - \cos(k_y a)], \quad (9)$$

which gives zero if the quasiparticle momenta are restricted to the nodes of a  $d_{x^2-y^2}$  gap. Using the terminology of Ref. 4, the nodes are inactive in the attenuation of all T1 phonons if only nearest neighbor interactions are considered. The inclusion of next-nearest-neighbor interactions would give finite attenuation of the T1 phonons. The next-nearest-neighbor interaction is expected to be relatively small [as is the case for  $\text{Sr}_2\text{RuO}_4$  (Ref. 15)], so the contribution of T1 phonons to electron-phonon heat transfer will be ignored. For the T2 phonons, Eq. (4) is used with quasiparticle momenta at the nodes to give

$$f^{T2}(\mathbf{q}, \mathbf{k}) = 2 \cos(\theta) \sin(\theta) [\cos(k_x a) \cos^2(\phi) + \cos(k_y a) \sin^2(\phi)], \quad (10)$$

which vanishes on the  $ab$  plane but for quasiparticle momenta at the nodes gives  $f^{T2}(\mathbf{q}, \mathbf{k}) = 2 \cos(\theta) \sin(\theta) \cos(k_x a)$  independent of  $\phi$  as was the case for longitudinal phonons. The attenuation of T2 phonons has the same  $\phi$  dependence as for longitudinal phonons. A plot to compare the attenuation of T2 phonons in the (101) and (111) directions, for example, would look the same as in Fig. 3.

### III. QUASIPARTICLE-PHONON HEAT TRANSFER

To calculate the heat transfer rate as a function of the electron and phonon temperatures, we integrate Eq. (2) over all phonon momenta and sum over independent modes. The velocity of sound appears in the phonon density of states and the electron-phonon matrix element, with the resulting heat transfer rate being proportional to  $1/c_s^5$ . Since longitudinal

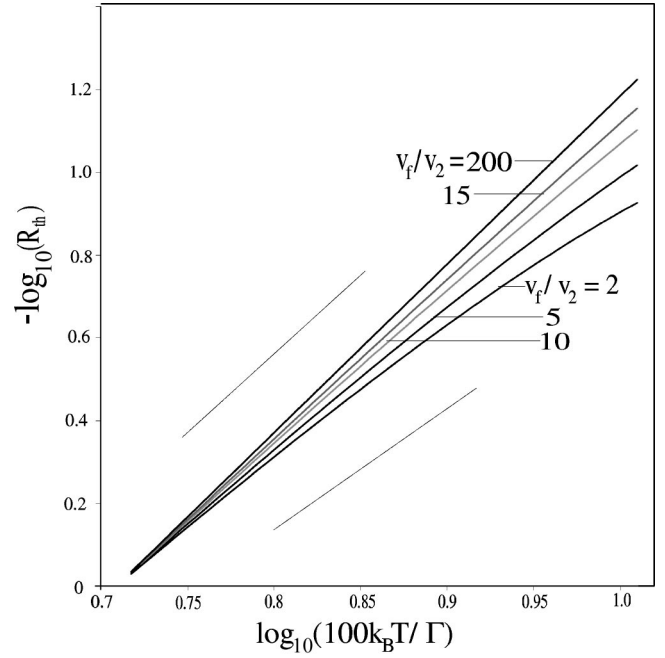


FIG. 4. A plot of  $\log(R_{th}\Omega)^{-1}$ , where  $R_{th}$  is the quasiparticle-phonon thermal resistance and  $\Omega$  the sample volume vs  $\log(100k_B T/\Gamma)$  for various values of the ratio,  $v_f/v_2$ . The lines above and below the curves show  $T^4$  and  $T^3$ , respectively. The magnitude of the thermal resistance depends on additional material parameters so the vertical scale is arbitrary, the curve intercepts have been adjusted for the graph. The temperature range extends from  $0.05\Gamma$  up to  $0.1\Gamma$ .

sound velocities are roughly a factor of 2 greater than transverse velocities, the heat transfer is dominated by the contribution of the T2 transverse phonons.

The heat transfer rate for a volume  $\Omega$  is found to be

$$\frac{dU}{dt} = \Omega K \int d(\hbar\omega) (\hbar\omega)^3 \left[ n \left( \frac{\hbar\omega}{k_B T_{ph}} \right) - n \left( \frac{\hbar\omega}{k_B T_{el}} \right) \right] F \left( \frac{\omega}{\Gamma} \right), \quad (11)$$

where

$$K = \frac{64n_p \hbar \Gamma^2 g^2 \cos^2(k_n a)}{\rho c v_f v_2 (\hbar c_s)^5 (2\pi)^5}, \quad (12)$$

and  $F(\omega/\Gamma)$  is obtained from integration of the phonon lifetime over  $\theta$  and  $\phi$ . The density of the sample  $\rho$ , the lattice constant  $c$  and the number of copper oxide planes in the unit cell  $n_p$ , appear in the expression.

The large value of the ratio  $v_f/v_2$  found in  $\text{YBa}_2\text{Cu}_3\text{O}_{6+x}$ ,<sup>3</sup> and used in the plots of Fig. 3, resulted in the strong anisotropy of the in-plane attenuation shown there. To observe the anisotropy of the attenuation crossover frequency with ultrasound measurements, unattainable frequencies of roughly  $0.1\Gamma = 3$  GHz would be required. The signature of the anisotropic attenuation may be seen in measurements of the quasiparticle-phonon heat transfer at millikelvin temperatures. This results from the fact that the

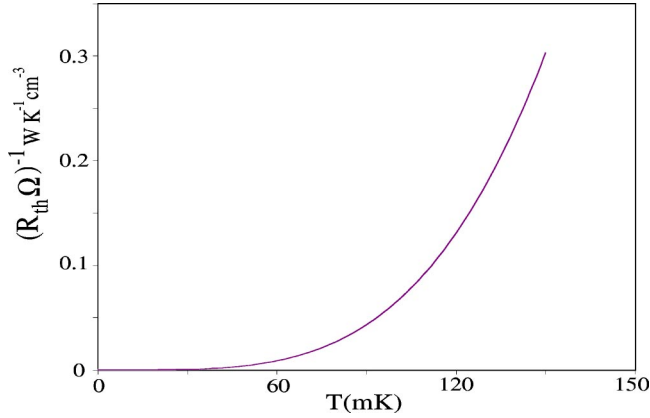


FIG. 5. The temperature dependence and approximate magnitude of  $(R_{th}\Omega)^{-1}$  for  $\text{YBa}_2\text{Cu}_3\text{O}_{6+x}$ . The true magnitude is obtained by multiplying this result by the square of the ratio of the electron-phonon coupling constant for  $\text{YBa}_2\text{Cu}_3\text{O}_{6+x}$  to that of  $\text{Sr}_2\text{RuO}_4$ . The quasiparticle-phonon heat transfer rate per unit volume is proportional to  $(R_{th}\Omega)^{-1}$  according to Eq. (14).

phonons which give the dominant contribution to the heat transfer at this temperature have frequencies in the range over which the crossover frequencies occur.

If the temperature difference  $T_{ph} - T_{el}$  is small compared to either  $T_{ph}$  or  $T_{el}$  then we can rewrite the heat transfer rate in terms of a thermal resistance. We take  $T_{ph} = T_{el} + \Delta T$  (henceforth  $T_{ph} = T$ ) and expand to first order in  $\Delta T$  to obtain

$$\frac{dU}{dt} = \Delta T / R_{th} = \Omega K (k_B \Delta T) (k_B T)^3 \int_0^\infty dx N(x) F\left(x \frac{k_B T}{\hbar \Gamma}\right), \quad (13)$$

where

$$N(x) = \frac{x^4 \exp(x)}{[\exp(x) - 1]^2}, \quad (14)$$

and  $R_{th}$  is the quasiparticle-phonon thermal resistance.

The function  $N(x)$  acts to restrict the frequency range which contributes to the integral in Eq. (14) according to the temperature. For temperatures well below  $0.01\Gamma$ , the contributing frequency range is strictly within the low-frequency limit in which the attenuation is proportional to  $\omega^2$  for all directions of sound propagation. The inverse resistivity  $R_{th}^{-1}$  is thus proportional to  $T^5$  according to Eq. (14). The temperature range expected in an experiment is significantly higher and would extend the range of contributing frequencies to roughly that displayed in Fig. 3. The resulting temperature dependence of the heat transfer rate depends on  $v_f/v_2$  as indicated in Fig. 4 in which  $\log(R_{th}^{-1})$  is plotted versus  $\log(k_B T/\Gamma)$  for several values of  $v_2$  using an experimental value for  $v_f$ .<sup>3</sup> The slopes of the curves shown in Fig. 4 indicate that the temperature dependence of the inverse resistance varies from roughly  $T^4$  behavior for  $v_f/v_2 = 200$

to a dependence which is close to  $T^3$  for  $v_f/v_2 = 2$ . The former ratio is close to that found for overdoped  $\text{Tl}_2\text{Ba}_2\text{CuO}_{6+\delta}$ ,<sup>25</sup> while the latter matches the value determined for underdoped  $\text{La}_{2-x}\text{Sr}_x\text{CuO}_4$ .<sup>26</sup> Both experimental values for  $v_f/v_2$  were obtained from low temperature thermal conductivity data.

The values of  $v_f$ ,  $v_2$ , and  $\Gamma$  can be extracted from transport measurements for many cuprate materials. If a measurement of the sound attenuation in a cuprate sample could be performed, then the magnitude of the quasiparticle-phonon thermal resistance could be determined. Since relatively large samples of certain cuprates are presently available, sound attenuation studies on these materials may soon be possible. With this in mind, we approximate the expected magnitude of the thermal resistance for optimally doped  $\text{YBa}_2\text{Cu}_3\text{O}_{6+x}$ . We use the value for the electron-phonon coupling constant,  $g = 12$  eV obtained for  $\text{Sr}_2\text{RuO}_4$ . Since the inverse thermal resistance is proportional to the square of the coupling constant, the magnitude of the inverse thermal resistance for  $\text{YBa}_2\text{Cu}_3\text{O}_{6+x}$  is equal to the result given below multiplied by the square of the unknown ratio of the coupling constants for the two materials. If this ratio is not substantially different from unity then the magnitude given here will be roughly correct. We take  $\hbar\Gamma = 1.5$  K, in agreement with the value extracted from thermal Hall measurements on  $\text{YBa}_2\text{Cu}_3\text{O}_{6+x}$ ,<sup>27</sup> and use values  $v_f = 2.5 \times 10^7$  cm/s and  $v_2 = 0.18 \times 10^7$  cm/s from thermal conductivity measurements.<sup>3</sup> The sound velocity for the T2 transverse mode is taken to be 3 km/s, in agreement with resonant ultrasound measurements of the elastic constants.<sup>20</sup> We then obtain the result for  $(R_{th}\Omega)^{-1}$  plotted in Fig. 5.

#### IV. CONCLUSIONS

We find for  $d$ -wave superconductors that the frequency above which sound attenuation no longer exhibits the  $\omega^2$  dependence characteristic of the low-frequency limit is highly anisotropic in the  $ab$  plane. Since the temperature dependence of the rate of energy transfer between phonons and quasiparticles is determined by the frequency dependence of the phonon attenuation rate, this temperature dependence should be expected to be significantly affected by the strong anisotropy in the crossover frequency. Our detailed calculations show that this is indeed the case. If the quasiparticle-phonon energy transfer rate calculated above can be detected, then the underlying planar anisotropy of the sound attenuation could be observed. A measurement of the heat transfer rate in a cuprate sample on which ultrasonic attenuation measurements could be performed would be most valuable. In this case, since the electron-phonon coupling constant could be obtained from the sound attenuation data, the magnitude of the heat transfer rate could be determined without any adjustable parameters. The predicted heat transfer rate could then be compared quantitatively with the experimental result.

We compare the temperature dependence of sound attenuation measurements made on  $\text{Sr}_2\text{RuO}_4$  (Ref. 16) in the hydrodynamic limit with the result that we calculate for superconducting order parameters having only vertical line nodes

(parallel to the  $c$  axis). We argue that the fact that the ratio of the attenuation of different longitudinal modes in the  $ab$  plane is independent of temperature is inconsistent with the presence of an order parameter which has vertical line nodes in the  $[110]$  or  $[100]$  planes. This fact can, however, be simply explained if the order parameter is taken to have horizontal line nodes. The experimental result for the attenuation of longitudinal sound modes in the superconducting state of

$\text{Sr}_2\text{RuO}_4$  thus provides evidence that the order parameter has only horizontal line nodes.

#### ACKNOWLEDGMENTS

We thank K. V. Samokhin, L. Taillefer, and J. Paglione for stimulating discussions, and acknowledge the support of the Canadian Institute for Advanced Research and of the Natural Sciences and Engineering Research Council of Canada.

- 
- <sup>1</sup>A. B. Pippard, *Philos. Mag.* **46**, 1104 (1955).  
<sup>2</sup>P. A. Lee, *Phys. Rev. Lett.* **71**, 1887 (1993).  
<sup>3</sup>M. Chiao, P. Lambert, R. W. Hill, C. Lupien, R. Gagnon, and L. Taillefer, *Phys. Rev. B* **62**, 3554 (2000).  
<sup>4</sup>J. Moreno and P. Coleman, *Phys. Rev. B* **53**, R2995 (1996).  
<sup>5</sup>F. C. Wellstood, C. Urbina, and John Clarke, *Phys. Rev. B* **49**, 5942 (1994).  
<sup>6</sup>M. E. Gershenson, D. Gong, T. Sato, B. S. Karasik, and A. L. Sergeev, cond-mat/0104083 (unpublished).  
<sup>7</sup>M. I. Kaganov, I. M. Lifshitz, and L. V. Tanatarov, *Zh. Éksp. Teor. Fiz.* **31**, 242 (1956) [*Sov. Phys. JETP* **4**, 173 (1957)].  
<sup>8</sup>W. N. Hardy, D. A. Bonn, D. C. Morgan, R. Lang, and Kuan Zhang, *Phys. Rev. Lett.* **70**, 3999 (1993).  
<sup>9</sup>J. A. Martindale, S. E. Barrett, K. E. Ohara, C. P. Slichter, W. C. Lee, and D. M. Ginsberg, *Phys. Rev. B* **47**, 9155 (1993).  
<sup>10</sup>K. A. Moler, D. L. Sisson, J. S. Urbach, M. R. Beasley, A. Kapitulnik, D. J. Baar, R. Liang, and W. N. Hardy, *Phys. Rev. B* **55**, 3954 (1997).  
<sup>11</sup>D. A. Wright, J. P. Emerson, B. F. Woodfield, J. E. Gordon, R. A. Fisher, and N. E. Phillips, *Phys. Rev. Lett.* **82**, 1550 (1999).  
<sup>12</sup>A. Hosseini, R. Harris, S. Kamal, P. Dosanjh, J. Preston, R. Liang, W. N. Hardy, and D. A. Bonn, *Phys. Rev. B* **60**, 1349 (1999).  
<sup>13</sup>M. B. Walker and M. F. Smith, *Phys. Rev. B* **61**, 1 (2000).  
<sup>14</sup>L. Taillefer, B. Lussier, R. Gagnon, K. Behnia, and H. Aubin, *Phys. Rev. Lett.* **79**, 483 (1997).  
<sup>15</sup>M. B. Walker, M. F. Smith, and K. V. Samokhin, *Phys. Rev. B* **65**, 014517 (2002).  
<sup>16</sup>C. Lupien, W. A. MacFarlane, Cyril Proust, Louis Taillefer, Z. Q. Mao, and Y. Maeno, *Phys. Rev. Lett.* **86**, 5986 (2001).  
<sup>17</sup>The linear response approach to the study of a sound wave propagating in the  $z$  direction in a crystal can be developed by attaching a fictitious charge to all atoms in the plane  $z=0$ , and applying to these  $z=0$ -plane atoms a fictitious homogeneous electric field of the correct frequency and polarization to generate the sound wave one wishes to study. This will generate sound waves propagating in the  $z$  direction in the region  $z>0$  of the crystal. Now, using the usual formulae of linear response theory, one finds that the thermodynamic average value of the oscillating displacement of an ion in the plane  $z=L$ , is given in terms of the single-particle phonon Green's function. From this, the given result can be derived.  
<sup>18</sup>I. Vekhter and E. J. Nicol, *Phys. Rev. B* **59**, 7123 (1999).  
<sup>19</sup>H. Won and K. Maki, *Phys. Rev. B* **49**, 1397 (1994).  
<sup>20</sup>Ming Lei, J. L. Sarrao, William M. Visscher, T. M. Bell, J. D. Thompson, A. Migliori, U. W. Welp, and B. W. Veal, *Phys. Rev. B* **47**, 6154 (1993).  
<sup>21</sup>J. Paglione, C. Lupien, W. A. Macfarlane, J. M. Perz, L. Taillefer, Z. Q. Mao, and Y. Maeno, *Phys. Rev. B* **65**, 220506 (2002).  
<sup>22</sup>M. C. Schabel, C.-H. Park, A. Matsuura, Z. X. Shen, D. A. Bonn, R. Liang, and W. N. Hardy, *Phys. Rev. B* **55**, 2796 (1997).  
<sup>23</sup>C. Bergemann, S. R. Julian, A. P. Mackenzie, S. NishiZaki, and Y. Maeno, *Phys. Rev. Lett.* **84**, 2662 (2000).  
<sup>24</sup>I. I. Mazin and D. J. Singh, *Phys. Rev. Lett.* **79**, 733 (1997).  
<sup>25</sup>C. Proust, E. Boaknin, R. W. Hill, L. Taillefer, and A. P. Mackenzie, *Phys. Rev. Lett.* **89**, 147003 (2002).  
<sup>26</sup>D. G. Hawthorn, M. L. Sutherland, R. W. Hill, C. Proust, C. Lupien, E. Boaknin, and L. Taillefer (unpublished).  
<sup>27</sup>Daniel Duffy, P. J. Hirschfeld, and Douglas J. Scalapino, *Phys. Rev. B* **64**, 224522 (2001).